Acta Biomaterialia 43 (2016) 218–229

Contents lists available at ScienceDirect

Acta Biomaterialia

journal homepage: www.elsevier.com/locate/actabiomat

Full length article

Mechanics of soft epithelial keratin networks depend on modular filament assembly kinetics

Joanna Deek, Fabian Hecht, Leone Rossetti, Katharina Wißmiller, Andreas R. Bausch *

Lehrstuhl für Zellbiophysik E27, Technische Universität München, James-Franck-Straße 1, 85748 Garching, Germany

ARTICLE INFO

Article history:
Received 3 March 2016
Received in revised form 4 June 2016
Accepted 9 July 2016
Available online 9 July 2016

Keywords:
Keratin
Networks
Phosphomimicry
Fluorescence microscopy
Electron microscopy
Rheology

ABSTRACT

Structural adaptability is a pivotal requirement of cytoskeletal structures, enabling their reorganization to meet the cellular needs. Shear stress, for instance, results in large morphological network changes of the human soft epithelial keratin pair K8:K18, and is accompanied by an increase in keratin phosphorylation levels. Yet the mechanisms responsible for the disruption of the network structure *in vivo* remain poorly understood. To understand the effect of the stress-related site-specific phosphorylation of the K8:K18 pair, we created phosphomimicry mutants – K8(S431E), K8(S73E), K18(S52E) – *in vitro*, and investigated the various steps of keratin assembly from monomer to network structure using fluorescence and electron microscopy, and using rheology characterized their network mechanical properties. We find that the addition of a charged group produces networks with depleted intra-connectivity, which translates to a mechanically weaker and more deformable network. This large variation in network structure is achieved by the formation of shorter mutant filaments, which exhibit differing assembly kinetics and a manifestly reduced capacity to form the extended structures characteristic of the wild-type system. The similarity in outcome for all the phosphomimicry mutants explored points to a more general mechanism of structural modulation of intermediate filaments via phosphorylation. Understanding the role of kinetic effects in the construction of these cytoskeletal biopolymer networks is critical to elucidating their structure-function properties, providing new insight for the design of keratin-inspired biomaterials.

Statement of Significance

Structural remodeling of cytoskeletal networks accompanies many cellular processes. Interestingly, levels of phosphorylation of the human soft epithelial keratin pair K8:K18 increase during their stress-related structural remodeling. Our multi-scale study sheds light on the poorly understood mechanism with which site-specific phosphorylation induces disruption of the keratin network structure *in vivo*. We show how phosphorylation reduces keratin filament length, an effect that propagates through to the mesoscopic structure, resulting in the formation of connectivity-depleted and mechanically weaker networks. We determine that the intrinsically-set filament-to-filament attractions that drive bundle assembly give rise to the structural variability by enabling the formation of kinetically-arrested structures. Overall, our results shed light on how self-assembled intermediate filament structures can be tailored to exhibit different structural functionalities.

1. Introduction

The keratin 8 (K8), keratin 18 (K18) pair is the cytoskeletal intermediate filament (IF) system found in soft epithelia [1–3]. Recent work has shown the K8:K18 system to be adaptable, with a time-dependent high turnover in the cell [1,3,4], and subject to multiple and site-specific post-translational modifications [5]. Of particular interest is site-specific kinase-dependent keratin phosphorylation, whose levels increase in periods of cell stress and mitosis, and is coupled to stages of the cell life-cycle that see large structural reorganization to its internal network components [6–9]. *In vivo* studies of phosphorylation-dependent IF structural change show a significant break in network homogeneity

Abbreviations: IF, intermediate filament; K8, keratin 8; K18, keratin 18; WT, wild-type; Ser/S, serine; Glu/E, glutamic acid; Ala/A, alanine; ULF, unit-length filament; TEM, transmission electron microscopy; STED, stimulated emission depletion.

* Corresponding author.
E-mail address: abausch@ph.tum.de (A.R. Bausch).

http://dx.doi.org/10.1016/j.actbio.2016.07.010
1742-7061/

throughout the cell, with regions of high protein density (with no observable mesh) and other IF-depleted regions [6–10].

The self-assembly of the K8:K18 pair [11–15], schematically depicted in Fig. 1a, begins with the necessary heterodimerization of the Type I K18 monomer with its pair-corresponding Type II K8 monomer. The heterodimers further assemble into tetramers, and the lateral association of four tetramers gives rise to the repeat denomination referred to as the Unit-Length Filament (ULF), Fig. 1a [11–15]. The longitudinal assembly of the ULFs creates the mature filament (diameter ≈ 10 nm), and the lateral association of mature filaments, driven by the presence of salt, creates the bundles of filaments [16–19], Fig 1a. The bundles further associate with one another, also by salt-mediated non-specific interactions and henceforth referred to as the crosslinks, forming the base physiological network structure observed within cells [4,20–22].

Previous work has shown that the non-helical domains of IF monomers play a role in subunit lateral alignment within filaments, filament elongation, and filament stabilization [18,23–25]. The localization of a phosphate group, generally within the head or tail domain of the monomers, has been found to affect the solubility, polymerization and network-forming propensities of the IF systems, with cases of hyperphosphorylation correlating to complete network collapse [4,9,10,26]. Serine (Ser, S) 431 of K8, for instance, is a basally phosphorylated site whose levels of phosphorylation increase during mitosis and with the increased expression of EGF-regulated-kinase [8]. Phosphorylation at Ser 73 of K8 (a substrate of p38 α-kinase) however, proceeds in an on/off manner [6]. In addition, K18 has also been found to be a substrate for kinases, with the most notable site corresponding to Ser 52 [7]. *In vivo* experiments on IF-depleted cells transfected with keratin

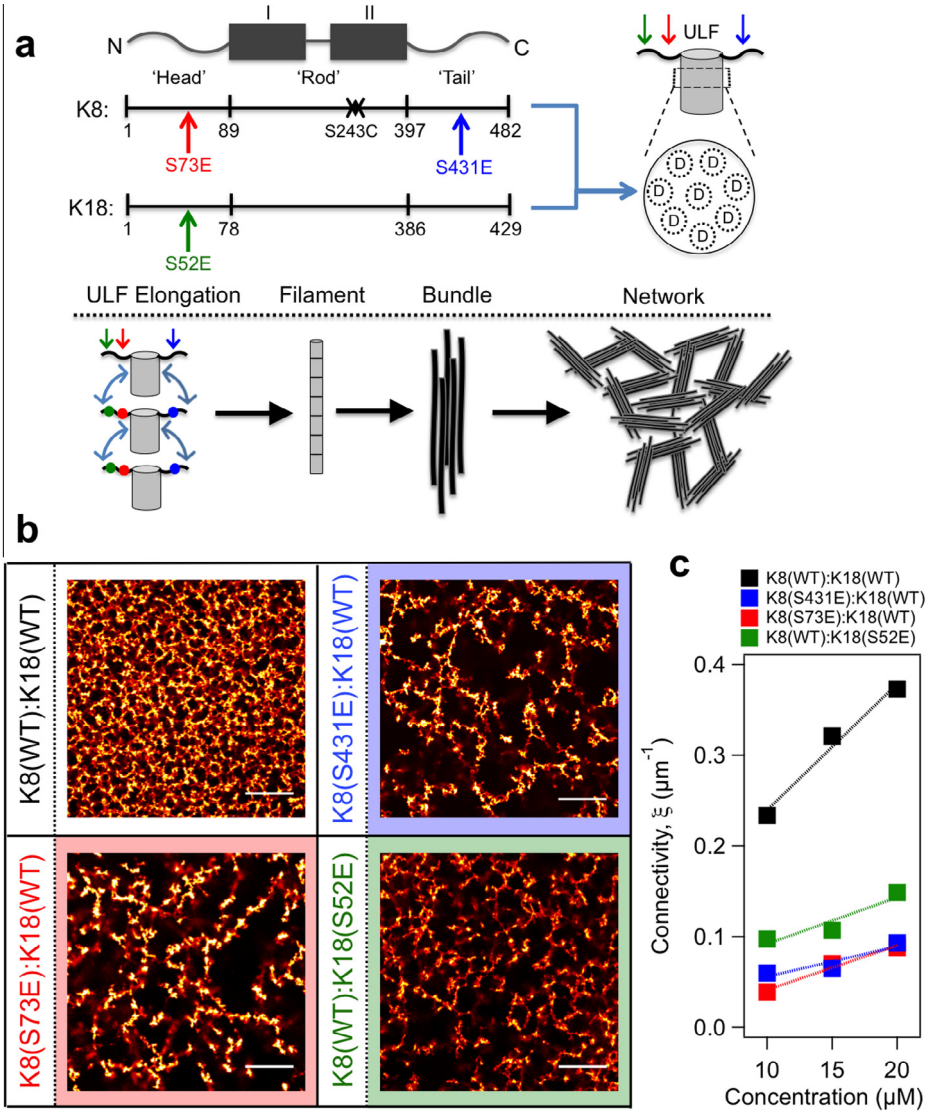

Fig. 1. Schematics of keratin monomers and network assembly, and structural variations between K8(WT):K18(WT) and phosphomimicry mutant networks. (a) Schematic representation of the keratin monomeric structure, with arrows marking the phosphomimicry mutation sites (numbering excludes the first methionine). Dimers (denoted as "D") are assembled from each of K8 and K18, and further associate to form the repeat unit – the unit length filament (ULF) – composed of 8 dimers in the lateral dimension. ULFs stack longitudinally, forming the mature filament; and the lateral association of the filaments drives bundle formation, which is the structural base of network formation (only 2 tails are schematically represented in the ULF, and omitted from the other structures for simplicity). (b) Confocal microscopy images of labeled keratin networks at 15 μM protein concentration highlight the significant structural impact of the introduced mutations, specifically in reducing network connectivity. Scale bar is 25 μm. (c) Graphical representation of network connectivity in μm^{-1} determined from confocal microscopy images of the various networks at the corresponding protein concentrations (for confocal images of the keratin networks at different protein concentrations, refer to Supplementary Figs. S1–S3). The network connectivity increases proportionally to the protein concentration, with that of the K8(WT):K18(WT) network being consistently larger (by ≈2-fold) than those observed for the phosphomimicry mutant systems. Error bars representing the fit result error for network connectivity, <0.005 μm^{-1}, are plotted in (c) but are smaller than their corresponding markers.

phosphomimicry mutants (created by replacing a native Ser with a Glutamic acid (Glu, E) residue, which is negatively charged at physiological pH) show that they produce seemingly normal networks and only display a disparity to the wild-type (WT) structure upon conditions of cellular stress [6,8]. Yet, what remains to be understood is the underlying mechanisms for structural rearrangements as a result of the phosphorylation.

Inspired by the observation of structural and functional disruption correlated to stress-related phosphorylation of the human epithelial keratin pair K8:K18 [6–8,10], phosphomimicry mutants – K8(S431E), K8(S73E), K18(S52E) – were created using site-directed mutagenesis, expressed, isolated and characterized. Confocal microscopy imaging shows the large structural variation between Ser → Glu networks and the WT counterparts, namely that the Ser → Glu mutants produce networks with reduced interconnectivity. The large similarity in features between the corresponding control Ser (S) → Alanine (Ala, A) mutants – K8(S431A), K8(S73A), K18(S52A) – and the WT system support the direct correlation between the addition of a phosphate group to the noted structural disruption. We show that the effect of added charge manifests as a shortening in filament length, thus producing connectivity-diminished networks with notably weaker mechanical strength.

2. Materials and methods

2.1. Keratin protein expression, isolation, and in vitro reconstitution

pET plasmids subcloned with the human K8 and K18 sequences were transformed into BL21 cells and expressed. Point mutations in the keratin sequences were made using the QuikChange Lightning Site-Directed Mutagenesis Kit (Agilent Technologies, Santa Clara, CA). The recombinant wild-type and mutant keratin proteins were expressed and purified as reported previously [12,16]. Purified K8 and K18 proteins were mixed in equimolar ratios in 8 M urea, 2 mM Tris-HCl (pH 9.0), 1 mM DTT, and renatured into 2 mM Tris-HCl (pH 9.0), 1 mM DTT – Low Tris (LT) buffer – by step-wise dialysis in 10 K MWCO devices (Pierce Biotechnology, IL, USA). At protein concentrations of ≈3 μM, mainly tetrameric complexes were found (by analytical ultracentrifugation) in LT buffer; but for concentrations of ≈13 μM, an increase in *s*-values indicated the onset of interaction between the tetramers at higher protein concentrations [13,15]. Using size-exclusion chromatography (discussed further in Sections 2.4 and 3.3), we find that at ≈20 μM in LT buffer, the keratin proteins are mainly in the ULF form. For experiments involving mature filaments or the network structure, protein solutions in LT buffer were subjected to a further dialysis step into Elongation buffer (EB) – 10 mM Tris-HCl pH 7.3 – producing elongated keratin filaments. The final protein concentration was determined after the final dialysis step by measuring the absorption at 280 nm using the Nanodrop ND-1000 (peqlab GmbH, Germany). All chemicals were obtained from AppliChem GmbH (Germany) and used without further purification.

2.2. Confocal and STED microscopy of keratin networks and image analysis

An additional mutation was incorporated in all of the K8 monomeric versions, K8(S243C), enabling the use of maleimide chemistry to couple the fluorescent dye Atto647N (ATTO-TEC, Siegen, Germany) to the monomers, performed according to the manufacturer's instructions. For all fluorescence microscopy measurements, a constant amount of 20% Atto647N-labeled K8 is incorporated into the sample (i.e. 10% sample-labeling), a labeling degree that does not disrupt the individual filament properties [16,27]. To image networks, protein filament solutions (either in LT or EB) were prepared to a final concentration of 10–20 μM in a 5 μL sample volume. The filament solutions were deposited onto microscope slides and polymerized into networks by the addition of 10X F-buffer (1 M KCl, 20 mM Tris-HCl (pH 7.5), 10 mM $MgCl_2$, 2 mM DTT), the "droplet-fusion" method as described elsewhere [16]. The confocal fluorescence imaging was conducted on a Leica SP5 confocal microscope (Leica Microsystems, Wetzlar, Germany). Mesh size and connectivity analysis was conducted using an Igor script, as discussed elsewhere [16]. Stimulated emission depletion (STED) fluorescence imaging of keratin networks was conducted on an in-house custom-built setup, as described elsewhere [28].

2.3. Electron microscopy of keratin single filaments and bundles

Keratin solutions were prepared for TEM and imaged as reported previously [11–13,15,16]. The LT-dialyzed protein solutions were incubated at room temperature (RT) then diluted to 4 μM in LT buffer. To image the single filaments, filament assembly was initiated by the addition of an equal volume of A-buffer – 18 mM Tris-HCl (pH 7.0) – to a 4 μM keratin solution in LT buffer. After ≈10 min of incubation at RT, the filament solution, now at 2 μM, was then mixed in a 1:1 ratio with fixation buffer (0.2% gluteraldehyde in A-buffer) to a final concentration of 1 μM protein. To image the bundles, assembly was initiated by the addition of an equal volume of B-buffer – 18 mM Tris-HCl (pH 7.2), 2 mM $MgCl_2$, 200 mM KCl [15] – to a 4 μM keratin solution in LT buffer and incubated at RT for ≈10 min, before the addition of an equal volume fixation buffer B (0.2% gluteraldehyde in B-buffer) to a final concentration of 1 μM protein. After gluteraldehyde fixation, protein samples were deposited onto glow discharged carbon-coated copper grids (Electron Microscopy Sciences, Hatfield, PA, USA) and negatively stained with uranyl formate. The electron microscopy was conducted on a Phillips CM100 transmission electron microscope (Philips/FEI Corporation, Eindhoven, Netherlands). Imaging was performed on all the keratin systems in both the Atto647N-labeled and the unlabeled form, with no significant differences observed. The contour length measurements were carried out using ImageJ. For statistical significance, the contour lengths of 50 randomly chosen filaments were manually traced using the built-in segmented line tool. Filaments only partially contained within the image were excluded from the analysis.

2.4. Monomer incorporation and self-assembly of wild-type and mutant keratins

The solubility and assembly competence of the WT and Ser → Glu monomers (i.e. the incorporation of monomers into the ULF and single filament structures) is investigated by sedimentation assays. To this effect, 20 μM keratin solutions in LT and in EB buffer were sedimented by low-speed centrifugation – 8000*g* for 30 min – and by high-speed centrifugation – 150,000*g* for 1 h. The post-sedimentation supernatants and pellets (dissolved in 8 M urea, 2 mM Tris-HCl (pH 9.0), 1 mM DTT) were run on 10% SDS-PAGE gels [17]. The sample compositions were determined by densitometry-analysis of the Coomassie-stained gels using ImageJ (U.S. National Institutes of Health, Bethesda, Maryland, USA).

Size-exclusion chromatography was run to determine the size distribution of assembled components in the LT buffer for all the keratin system pairs. Renatured keratin pair protein solutions at 20 μM in LT were sedimented at 10,000*g* at room temperature for 10 min. The supernatants were loaded onto a Superose 6, 10/300 GL column (GE Healthcare Bio-Sciences, Sweden), pre-equilibrated in LT buffer, and run in LT buffer. The elution profile was monitored and fractions collected. The fractions were polymerized by the addition of 10X F-buffer, sedimented (150,000*g* at

room temperature for 1 h), and the urea-dissolved pellets (using 8 M urea, 2 mM Tris-HCl (pH 9.0), 1 mM DTT buffer) run on 10% SDS-PAGE gels, with sample compositions determined as stated above.

2.5. Rheology of keratin networks

Rheology measurements were conducted on a stress-controlled rheometer (Physica MCR 301; Anton Paar) using the 25 mm cone-plate geometry (with a 50 μm gap size at the center of the cone). The EB-dialyzed keratin filament solutions, concentration-adjusted and at RT, were deposited at the center of the bottom plate. One-tenth the sample volume in F-buffer was distributed (in 1 μL aliquots) around the circumference of the bottom of the cone surface. After joining both plates, the sample was given one hour to equilibrate before the measurements' start (polymerization curves confirm that after one hour the sample is fully equilibrated, whereby the $G'(\omega)$ no longer changes, data not shown). A solvent trap was placed around the sample to prevent drying artifacts, and measurements were conducted at 21 °C. The viscoelastic response of equilibrated keratin networks was determined by measuring the frequency-dependent storage modulus $G'(\omega)$ and loss modulus $G''(\omega)$ over a frequency range of three decades. To ensure a linear response, and as confirmed by preliminary amplitude sweeps, small torques (≈0.5 μNm) were applied. The resulting G' and G'' at 1 rad/s were used to compute the phase angle ($\delta = \tan^{-1}(\frac{G'}{G''}) \times \frac{180^\circ}{\pi}$), reflecting the relative viscous and elastic network components. The non-linear keratin network response, the stress-strain $\sigma(\gamma)$ relation, was investigated at the strain rate, $\dot{\gamma} = 1.25\%\text{s}^{-1}$. The stress-strain curves were smoothed, and the differential modulus $K(\gamma) = \frac{\partial \sigma}{\partial \gamma}$ calculated [29,30].

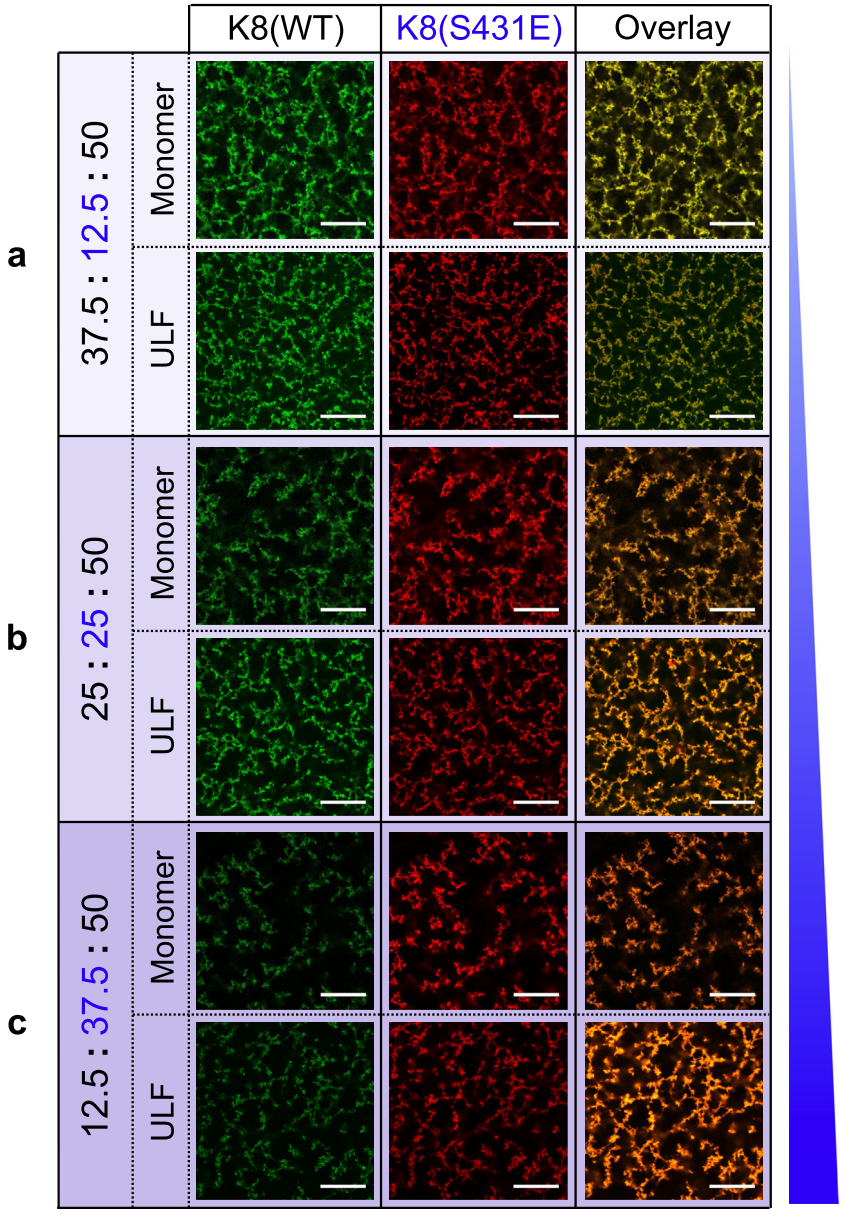

Fig. 2. Two-channel confocal microscopy images of double-stained K8(WT):K8(S431E):K18(WT) networks for varying ratios of K8(WT):K8(S431E). 20% of each of the K8 monomers is fluorescently-labeled: K8(S431E) with Atto647N, and K8(WT) with Atto488. The networks (at 20 μM) are assembled in two separate fashions, with "Monomer" referencing the mixing of the three monomer types (K8(WT), K8(S431E), K18(WT)) in 8 M urea prior to the step-down dialysis, and "ULF" denoting the mixing of the two ULF types (K8(WT):K18(WT) and K8(S431E):K18(WT)) in LT buffer prior to network formation. The complete colocalization of both dyes is observed for all the K8(WT):K8(S431E):K18(WT) compositions of (a) 37.5:12.5:50, (b) 25:25:50, (c) 12.5:37.5:50, in addition to a gradual loss in connectivity correlating to the ratio increase of K8(S431E). Scale bars are 25 μm.

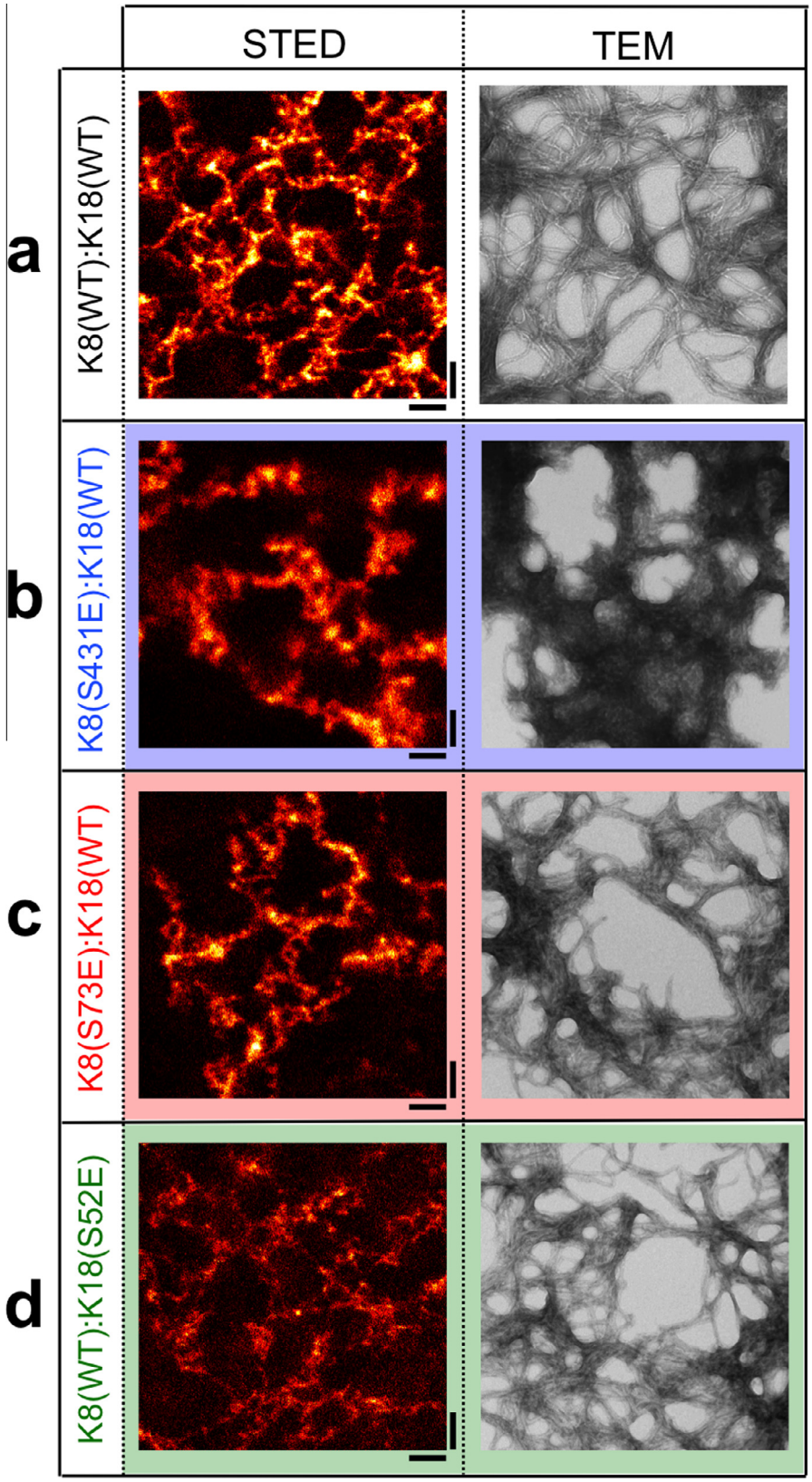

Fig. 3. STED and electron microscopy images of bundles within keratin networks. Microscopy images of networks of Atto647N-labeled (a) K8(WT):K18(WT), (b) K8(S431E):K18(WT), (c) K8(S73E):K18(WT), (d) K8(WT):K18(S52E) at 20 μM protein concentration in STED mode (left column), and further fixed for electron microscopy imaging (right column). Bundles of the WT system are made of extended, thread-like components, in contrast to the Ser → Glu counterparts that are more stocky in appearance, and less uniform in size. Interestingly, the characteristic clustered appearance revealed using fluorescence microscopy is also mirrored in the increased dimensionality of the Ser → Glu structures observed with TEM, with (b) K8(S431E):K18(WT) presenting the most extreme phenotype. The stunted bundles appear to sterically confine their subsequent higher-order structures to a much lesser extent, and thus giving rise to the observed node-like structures. TEM also reveals the sub-bundle filament arrangement, seemingly organized of shorter Ser → Glu filaments relative to the WT system. STED images are 10 μm × 10 μm, and TEM images are 1 μm × 1 μm (black bars at the bottom-right of the STED images, also 1 μm, added as a reference to the relative sizes).

2.6. Statistical analysis

The mesh size analysis of the confocal images was done using an in-house Igor Pro script, as previously described [16]. The error is estimated by the standard error of the least squares fit. The contour length of the filaments observed using TEM was estimated using the ImageJ "Segmented Line Tool" (U.S. National Institutes of Health, Bethesda, Maryland, USA). The statistical analysis of the contour length results was done in Igor 6 Pro, and with n = 50 for each keratin system pair, reported as the sample median ($\tilde{x}$), and the arithmetic mean ($\bar{x}$) with its corresponding error ($SE_{\bar{X}}$). The data obtained from the rheology measurements were averaged and expressed as means ± standard deviations.

3. Results

3.1. Structural variation between mutant and wild-type networks

The wild-type keratin pair K8(WT):K18(WT) and the corresponding phosphomimicry mutant pairs – K8(S431E):K18(WT), K8(S73E):K18(WT), and K8(WT):K18(S52E) – are assembled and then elongated into mature filaments. The subsequent addition of salt drives filament bundling, which also coincides with network formation. Confocal microscopy images of networks of the fluorescently-labeled Ser → Glu keratin pairs, depicted in Fig. 1b, reveal a significant loss in network connectivity compared to the K8(WT):K18(WT) system. This reflects a mutation-dependent change in the framework that underlies the final network structure.

We define the network mesh as the observed inter-bundle void, which is the inverse of the inter-bundle connectivity, and report the quantified connectivity in μm^{-1} as a function of the initial keratin protein concentration, Fig. 1c. The trend of increasing connectivity with protein concentration is clearly reflected in all keratin pairs, whereby the connectivity of the Ser → Glu mutants is at least twofold smaller than that for the WT at all concentrations. But, the change in network connectivity for the Ser → Glu mutants is significantly less dependent on the protein concentration in comparison to the WT networks. A doubling in protein concentration from 10 μM to 20 μM approximately doubles the network connectivity in the WT system, as opposed to increasing the connectivity by less than 20% for all the Ser → Glu mutant systems.

An investigation of the corresponding control Ser → Ala mutants (Supplementary Figs. S1–S3) substantiates the correlation between structural disruption and the presence of the charged amino acid, as expected for a native phosphorylation site: features of Ser → Ala mutant networks are very similar to those of the WT, excluding the possibility that mutating the Ser residue alters the ability of the protein to properly assemble. Nevertheless, the slightly looser mesh of the Ser → Ala mutant networks (with reference to the WT networks) points to the presence of a sequence-specific association component.

As previously demonstrated [16], the initial keratin concentration dictates the final keratin network mesh features, whereby the higher the initial protein concentration (i.e. the higher the abundance of filaments), the more prevalent the interconnectivity of the constituent elements, and the smaller the resultant network mesh. The route-dependence of the network properties highlights the non-equilibrium arrested nature of the network formation of the K8:K18 pair. Furthermore, the observed mesh size for K8(WT):K18(WT) bundled networks at 20 μM is ≈3 μm, much larger than the <0.5 μm measured for networks of keratin filaments [29]. The significantly looser mesh observed in the bundled networks suggests that the final arrested network arrangement is determined by more than simple diffusion, and is driven by the interfilament interactions that promote the formation of the larger assembly structures.

Confocal microscopy experiments on double-stained ternary K8(S431E):K8(WT):K18(WT) networks – K8(S431E)_#Atto647N and K8(WT)_#Atto488 – map the dose-dependent effect of mutant incorporation into the network structure, Fig. 2. K8(S431E) and K8(WT) monomer assembly sample mixes (with K18(WT)) form identical networks to sample mixes of their corresponding independently-assembled ULFs. Network connectivity was reduced with the increasing K8(S431E) to K8(WT) ratio. The colocalization of both dyes demonstrates an equal likelihood for both K8(S431E) and K8(WT) monomers, as well as the corresponding ULFs they each form in combination with K18(WT), to be incorporated into the final structure. The ratio-dependent loss in connectivity substantiates the Ser → Glu mutant's effect in altering the kinetics of assembly of filaments and bundles into networks, thus resulting in the differing outcomes of their structural arrest. We propose that the main determinant of final network structure is a kinetic arrest component within the network assembly scheme, driven by filament-to-filament interactions. We predict that the Ser → Glu mutation changes the constituent features such that they construct varied arrested structures upon assembly.

3.2. Mutant-dependent change of bundle features

Given a network construct based on filament-to-filament interactions, and the observation that the Ser → Glu mutants arrest into networks with notably reduced interconnectivity (Fig. 1b), the variability between the mutant and the WT bundle structures must be the basis for the different arrest structures. We investigate the bundle structures of the K8(S431E):K18(WT), K8(S73E):K18(WT), and K8(WT):K18(S52E) keratin networks, and compare them to the K8(WT):K18(WT) system. STED microscopy enables us to image the bundles and how they associate within their networks, and TEM to observe their features that are further beneath the resolution limit of fluorescence microscopy, Fig. 3. STED imaging of the networks at 20 μM reveals the bundle (and bundle-to-bundle association) morphologies with a resolution of ≈70 nm, as compared to ≈200 nm for confocal microscopy (Supplementary Fig. S4). The most striking distinction is that the WT structures appear to be more string-like and spatially-extended, as opposed to the nodes characteristic of the Ser → Glu networks. Unlike the regularity of the WT bundle-to-bundle interaction, the Ser → Glu bundles associate into less ordered structures. The clustered domains of Ser → Glu bundles do not grow indefinitely, reinforcing our findings that the bundle formation is not aggregation-driven, but rather results from preset filament lateral association. Thus the structural difference between WT and Ser → Glu lies in the allowable conformations for bundle-to-bundle associations, with the Ser → Glu formations resulting from less constrained bundle interaction and growth.

TEM reveals the internal arrangement of bundles, and based on their structures and sizes, we can clearly deduce that those observed using confocal and STED microscopy were bundle-to-bundle assemblies. The TEM observations of the WT system reflect the string-like and spatially-extended conformation as seen with the STED. On the other hand, the multi-layered and irregular structures show how Ser → Glu bundles are less restricted than their WT counterparts in their mode of association, where with lesser control for their further association in the lateral direction, the bundles grow into more branched arrangements. By this we demonstrate that the assembly involving shorter bundles, which have a higher propensity to make irregular (branched) bundle-to-bundle associations, produces a less entangled network with reduced interconnectivity. The variation in WT and Ser → Glu bundle-to-bundle association is additional evidence for the arrest

component in the building of the network. The longer-range of the WT bundles, in contrast to the Ser → Glu bundles, conveys that the arrested constructs, with self-set steric accessibility, are the scaffold for further growth. This means that because of their more expansive conformational arrangement, and thus the higher steric limitation created by their arrested constructs, the WT system forms more affine network structures. On the other hand, the shorter Ser → Glu bundles do less to restrict the modes of further

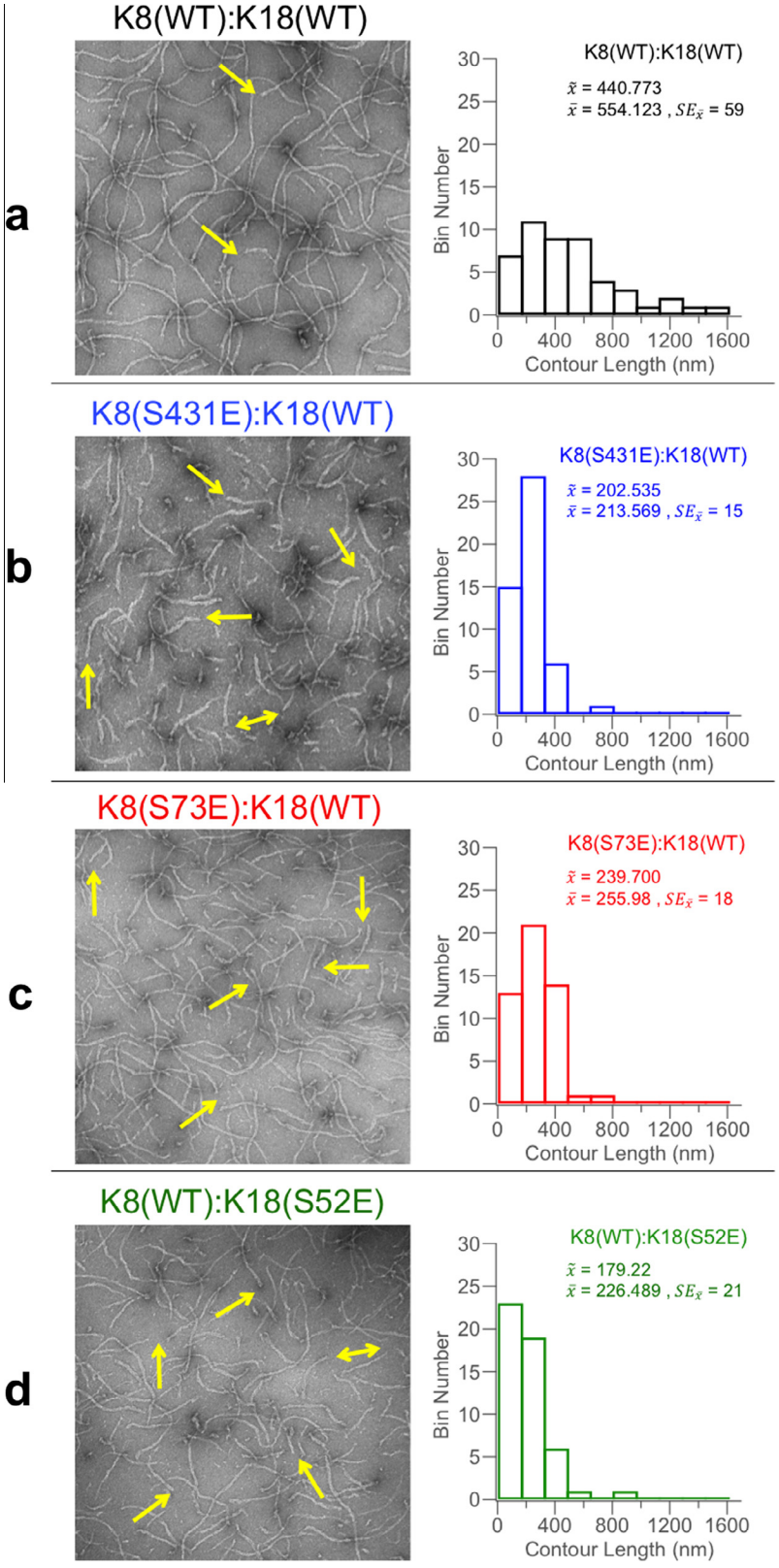

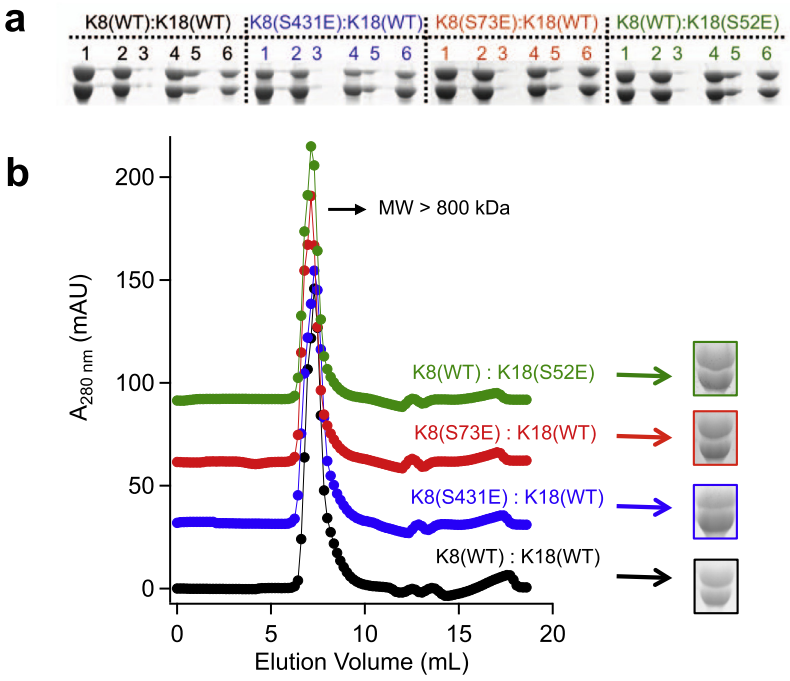

Fig. 5. Monomer incorporation into assembled structures. (a) Coomassie-stained 10% SDS-PAGE of the low-speed sedimentation assay: 1 = sample stock in 8 M urea buffer, 2 = supernatant of Low Tris buffer sample, 3 = pellet of Low Tris buffer sample, 4 = supernatant of Elongation buffer sample, 5 = pellet of Elongation buffer sample, 6 = pellet of F-buffer sample. The composition in all lanes (i.e. ratio of K8 to K18) remains constant under all buffer conditions, showing that all the K8 monomers form their corresponding dimer with the K18 monomers. Equivalent results for lanes 2 and 3 for all the system pairs confirm an equal incorporation of the K8 Ser → Glu mutant monomers – K8(S431E) and K8(S73E) – and K18(S52E) with K8(WT) and K18(WT), respectively, into the soluble dimer, tetramers, and/or ULFs. There is no apparent variation in filament bundling tendency for the different keratin combinations, as depicted by the comparable protein distribution between lanes 4 and 5, with 15 wt% sedimenting for all system pairs (lane 5, the pellet). (b) Elution profiles for the WT and phosphomimicry K8:K18 pairs using a Superose 6 10/300 GL column. The K8(WT):K18(WT), K8(S431E):K18(WT), K8(S73E):K18(WT), and K8(WT):K18(S52E) pairs are each assembled at 20 μM in LT buffer. The system pairs are each separated using a Superose 6 10/300 GL column, and the corresponding elution profiles are plotted. The elution profiles of all the system pairs are identical, with one prominent peak corresponding to the ULFs of MW ≈800 kDa. The absence of other significant peaks, especially for the phosphomimicry systems, clearly demonstrates that the monomers fully assemble into ULFs and do not get trapped in smaller assembly structures (e.g. dimers, tetramers). The fractions corresponding to each of the prominent peaks were pooled, polymerized by the addition of F-buffer, sedimented, and the pellets run on a 10% SDS-PAGE gel. The gel results again show the 1:1 ratio of K8:K18 incorporation.

association, enabling clustering and thus producing the lesser connected nodes. Furthermore, and based on the internal filament arrangement observed in the TEM images, the Ser → Glu mutant filaments appear to be shorter than the WT filaments. These findings suggest that given the same propensity for lateral filament-to-filament association, the shorter filaments would also assemble into shorter bundles, and thus produce the less-expansive arrested structures observed with confocal and STED microscopy.

3.3. Monomer incorporation into assembled structures, and filament properties

We use TEM to image the fixed and elongated filaments for the WT and the Ser → Glu mutant system pairs to confirm the observation that the Ser → Glu mutant filaments that assembled into bundles are shorter than the WT filaments, Fig. 4. As expected, the K8(S431E):K18(WT), K8(S73E):K18(WT), and K8(WT):K18(S52E) system pairs assemble into ≈10 nm thick filaments, identical to the K8(WT):K18(WT) pair, albeit shorter. Interestingly, the K8(S431E) mutation also appears to affect the filaments' ability to exhibit the minor radial reorganization ("compaction") otherwise observed for the WT system [13]. For the Ser → Glu mutants, the number of filament ends per area is much larger than that for the WT filaments. An estimate of filament contour length, based on statistics from 50 filaments per system pair (source TEM images presented in Supplementary Fig. S5), quantifies the median ($\tilde{x}$) length difference at ≈440 nm for the WT system, and ≈200 nm for the Ser → Glu mutants, Fig. 4. The findings corroborate the prediction that the WT filaments are longer, measuring at approximately twofold the length, than those formed by the Ser → Glu mutants.

To exclude the possibility that the reduced mutant filament length is due to diminished monomer incorporation into assembled components, the assembly of Ser → Glu monomers into ULFs and filaments is investigated. Samples in each of LT buffer (ULFs), E-buffer (elongated filaments), and F-buffer (bundles and network) are centrifuged at very low speeds, and the results of this sedimentation assay presented in Fig. 5a. Over 95% of the sample in LT

Fig. 4. TEM images of negatively-stained keratin filament system pairs and their corresponding length analysis. (left column) TEM images of the fixed keratin filaments – given the same elongation time at fixed buffer conditions (10 mM Tris, pH 7.3), and prepared at 1 μM – and (right column) their corresponding length analysis are presented. (left column) The results reveal that the (b) K8(S431E):K18(WT), (c) K8(S73E):K18(WT), and (d) K8(WT):K18(S52E) system pairs have a comparable diameter, but are notably shorter than their (a) K8(WT):K18(WT) counterparts. For the Ser → Glu mutants, the number of filament ends per area (few ends pointed-to with yellow arrows as a guide to the eye) is much larger than that for the WT filaments. (right column) The filament contour length analysis was conducted on the lower-magnification TEM images of the negatively-stained system pairs, depicted in Supplementary Fig. S5, with n = 50 for each pair, and reported as the sample median ($\tilde{x}$), and the arithmetic mean ($\bar{x}$) with its corresponding error ($SE_{\bar{x}}$). Contrary to the narrow range of contour length measurements for the Ser → Glu mutants, the WT system exhibits a much larger data spread, making the $\tilde{x}$ the better representative for average filament contour length. The K8(WT):K18(WT) filaments have an estimated median contour length of ≈440 nm, which is 2-fold longer than that estimated for any of the Ser → Glu filaments, ≈200 nm. Each TEM image is 1 μm × 1 μm.

buffer is retained in the supernatant, with no distinction between the Ser → Glu and the WT system pairs. The absence of a pellet, which would otherwise be composed of misfolded proteins (single type monomers have poor solubility and sediment upon centrifugation – data not shown here), signifies the full incorporation of all monomers into soluble dimers and/or multimers. Size-exclusion chromatography on all the keratin pairs in LT buffer, Fig. 5b, with a single prominent peak emerging at MW ≈ 800 kDa, the expected MW of a 16-mer, confirms that monomers for all the observed system pairs are equally assembled into the ULF form.

Exchanging the sample buffer from LT to E-buffer results in filament formation. Again, the similarity in sedimentation behavior observed for both the Ser → Glu and the WT system pairs, Fig. 5a, *with* ≈15% of the sample sedimenting on centrifugation, excludes the possibility that the mutations may act to change the bundling tendency of the resultant filaments, as has been observed with more severe EBS-type mutations [32]. This also correlates with the observation of no change in sample viscosity upon exchange into E-buffer, otherwise characteristic of filament bundling and concomitant network formation. High-speed sedimentation of the samples in E-buffer display an almost complete sedimentation of all keratin pairs, with no distinction between the Ser → Glu and the WT, confirming the elongation of all ULFs into filaments, Supplementary Fig. S6. And finally, in F-buffer all system pairs are fully gelled, with no supernatant and pellet phase separation, and exhibit the expected 1:1 network composition, Fig. 5a.

Thus, by identifying the equal incorporation of Ser → Glu and WT monomers into all assembled structures, we demonstrate that the added charge reduces average filament length, and underscores the correlation between component length and the morphology of the final arrested network structure.

3.4. Impact of mutation-induced structural changes on network mechanical properties

Since the mutations' impact is a reduction in network connectivity, the expectation is that they form mechanically weaker networks. Using rheology, we report on the mechanical properties of the K8(S431E):K18(WT), K8(S73E):K18(WT), and K8(WT):K18(S52E) keratin networks, and compare them to the K8(WT):K18(WT) system, Fig. 6. The keratin pairs are elongated into filaments (in EB), and then assembled into networks between the rheometer plates by the addition of salt. The linear response rheological elastic (G′) and viscous (G″) moduli for the WT and Ser → Glu keratin pairs at all concentrations measure G′ values at approximately 10-fold the G″ values, Fig. 6a, as expected for crosslinked systems. The measured G_0 values, ≈1–10 Pa, increase in correlation to protein concentration, and thus interconnectivity, for all systems. Nevertheless, the Ser → Glu mutant systems are considerably weaker, attributed to fewer inter-connections, with ≈2-fold lower G′ and G″ values for all protein concentrations probed. The phase angle, δ, computed using G′ and G″ values in the frequency-independent regime (see Section 2), numerically reflects the relative viscoelasticity of the network (with the larger value reflecting a more significant viscous component), Fig. 6b. The results show the Ser → Glu systems to be more viscous than the WT system at all concentrations.

To test their nonlinear response, the keratin networks are then subjected to a gradual increase in strain (γ), at the strain rate $\dot{\gamma} = 1.25\%s^{-1}$, and the corresponding stresses (σ) measured. Plots of the differential modulus, K(γ), show keratin's characteristic strain-stiffening behavior (Supplementary Figs. S7 and S8), with the range for the linear response (attributed to filament stretching, and independent of keratin protein concentration) at $\gamma \approx 10\%$, as observed elsewhere [29,33]. The yield stress (σ_{yield}), Fig. 6c, and the yield strain (γ_{yield}), Fig. 6d, are the stress and strain values

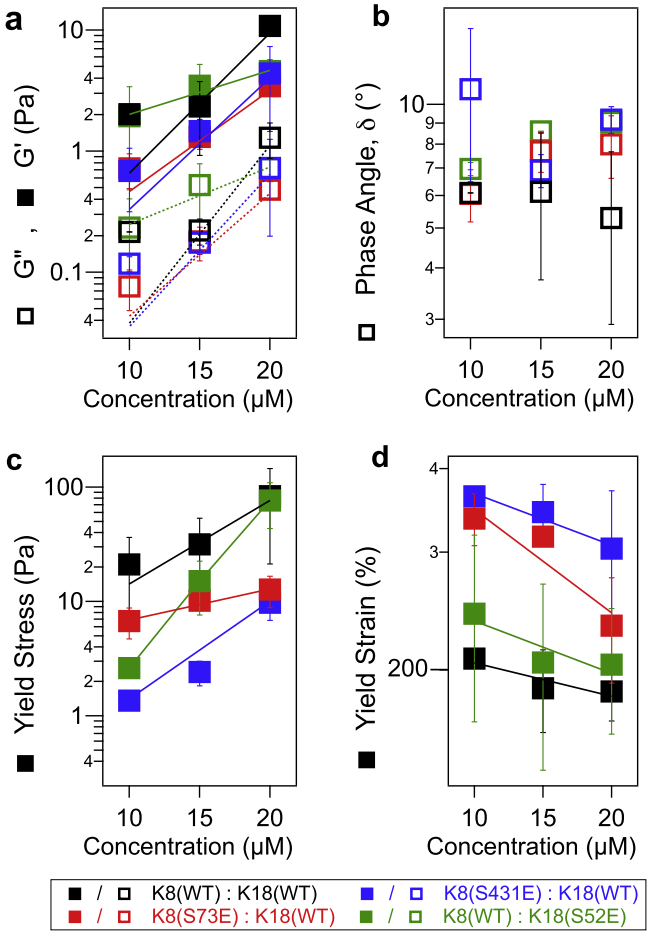

Fig. 6. Mechanical properties of K8(WT):K18(WT) networks and their phosphomimicry mutants. (a) The elastic and viscous moduli of the networks, obtained from the corresponding frequency sweeps at 1 rad/s, increase with increasing protein concentration. In all systems, the G′ is approximately 10-fold the measured G″ values, as expected for crosslinked networks. The WT network, exhibiting the largest degree of connectivity, is also the most elastic of the keratin network combinations. (b) Quantifying the phase shift between the networks' elastic and viscous components (reported in (a)) as a function of protein concentration, we note an increase in the viscous component of the mutant networks compared to the WT, correlating with the reduction in network connectivity. (c) Analysis of stress-strain curves of the keratin networks ($\dot{\gamma} = 1.25\%s^{-1}$) demonstrates the ability of the WT network to dissipate significantly more stress than the Ser → Glu mutant networks. The dissipative ability also increases with protein concentration, as would be expected due to the increase in constituent connectivity associated with a higher volume fraction of protein filaments. (d) Interestingly, the yield strain is consistently larger at all points for the Ser → Glu mutants than that for the WT network, reflecting the higher deformability of the mutant networks that exhibit looser connectivity (please refer to Supplementary Fig. S7 for representative stress-strain curves of the WT and Ser → Glu networks, and Supplementary Fig. S8 for representative profiles of the corresponding Ser → Ala mutants). Error bars are the standard deviation of multiple measurements, with n ⩾ 2 for each reported value, and the linear fits are intended to guide the eye.

respectively at which the networks fail. The σ_{yield} increases with protein concentration, and for the WT networks is higher than that for the Ser → Glu mutants, consistent with the expectation for more extensively crosslinked networks. Conversely, γ_{yield} is significantly lower for the WT networks, reflective of the notably higher deformability of the Ser → Glu networks. This is consistent, not only due to the dampened connectivity, but also in light of the higher viscosity of the Ser → Glu networks.

The reduction in filament length, responsible for producing the varied bundle structures with diminished interconnectivity, effectively assembles weaker and more deformable networks. The G_0 values compare to those previously measured for bundled

K8(WT):K18(WT) systems [34], and exhibit a stronger concentration-dependence as well as a markedly higher σ_{yield} than non-bundled filament networks at comparable protein concentrations [29,33]. The findings demonstrate that bundling adds further control/modularity to the system, enabling another level of mechanical control via changes in crosslinker number as a function of concentration. Additionally, it is plausible that phosphorylation is also accompanied by a reduction in filament persistence length, due to the mutants' lower ability to stabilize the vertical stacking of the ULFs. This effect could further translate to a weakening in individual bundle strength, which is a function of the persistence length of the constituent filaments [20].

4. Discussion

This combinatorial *in vitro* investigation sheds lights on previously unexamined features of phosphorylation-dependent K8:K18 network structural changes, notably in the absence of associated proteins. Using phosphomimicry mutants, we map the effect of the Ser → Glu mutation at the various assembly stages and how it propagates to the various levels of structure in the keratin network, ultimately altering the network mechanical properties. We show that the result of adding a charged amino acid is primarily manifested as filament shortening, a phenomenon also reported for other types of disease-associated mutations of IF systems [24,35]. TEM imaging on elongated filaments depicts that the studied Ser → Glu mutations act to reduce median filament length from ≈440 nm for the WT to ≈200 nm for the Ser → Glu mutants. This observed difference in filament length provides evidence for the tuning of filament elongation dynamics, in line with *in vitro* work that has implicated the head and tail domains in stabilizing filament elongation [18,23–25].

As seen using confocal and STED microscopy, the shorter Ser → Glu mutant filaments assemble into a connectivity-depleted network of often-disconnected protein bundle nodes. This characteristic node-like structure of the Ser → Glu mutant networks strikingly resembles the modeled network construct variation resulting from a twofold reduction in constituent filament length [31]. For a system of filaments driven by long-range filament-to-filament attractions, Kim et al. [31] predict that shorter filaments sequester into dispersed filament clusters, producing a predictably less elastic network due to the reduced number of crosslinks for comparable numbers of filament pairs. And that on the other hand, increasing the filament length produces larger crosslinked networks [31]. In addition to demonstrating experimentally the correlation between filament length and network connectivity, we show that filament-to-filament interactions are sufficient to drive keratin bundle and network formation.

The Ser → Glu mutant-induced network structural disruption can be observed as a result of either monomer or ULF incorporation, implying that the structural changes ensuing from phosphorylation are independent of the keratin assembly stage. This observation can be correlated to cellular mechanisms of network reformation and disruption, and is in agreement with post-assembly network modulation and the turnover model of keratin in the cell [4].

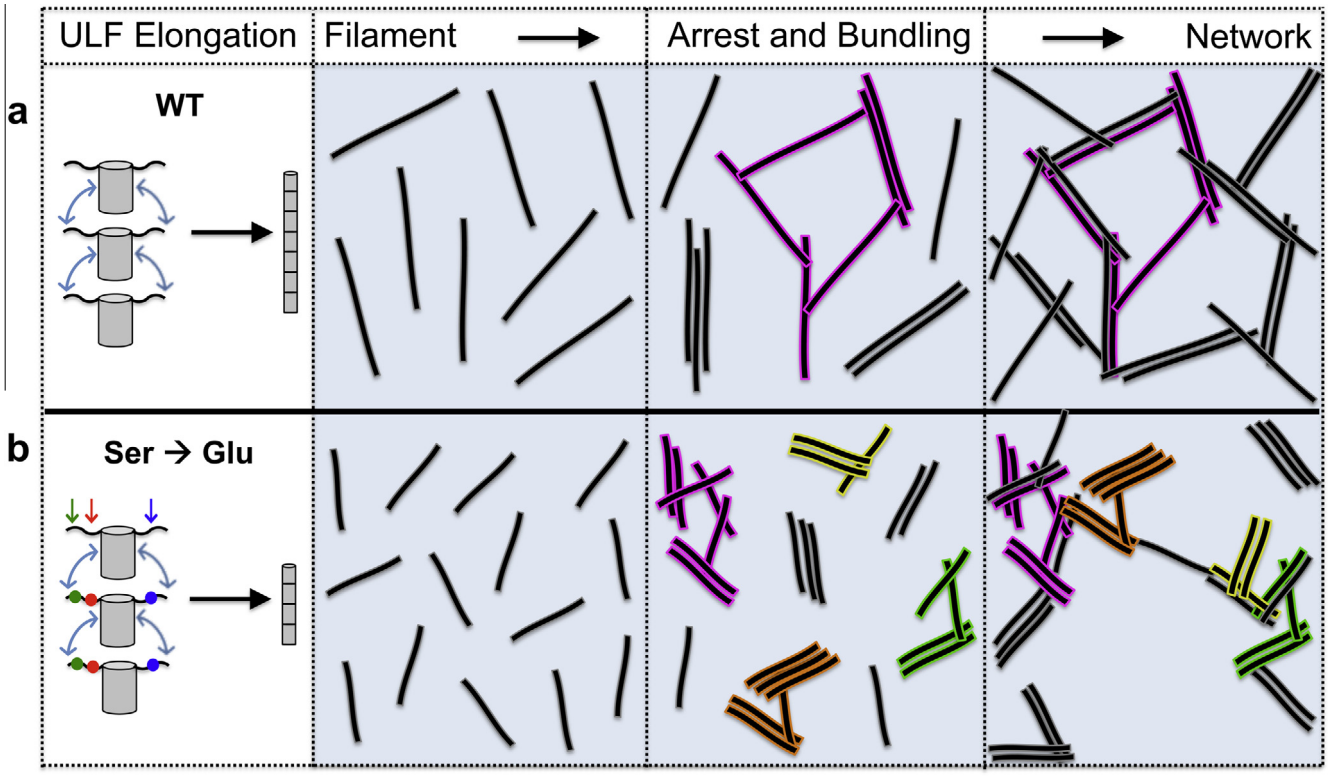

Fig. 7. The effect of monomer phosphorylation translated to the various stages of assembly of the K8:K18 pair. In both the (a) K8(WT):K18(WT) and the (b) K8(S73E):K18(WT)/K8(S431E):K18(WT)/K8(WT):K18(S52E) pairs, self-assembly begins with the vertical stacking (elongation) of the ULFs, forming the mature filament (d = 10 nm). For the (a) K8(WT):K18(WT) system, filament length measures on the order of 400 nm; on the other hand, (b) filaments of phosphorylated monomeric components are found to be significantly shorter in length, ≈200 nm. Upon addition of salt, the self-association of filaments, which simultaneously produces both bundles and arrested structures, results in network formation. The color-contoured filaments in the third column highlight such arrested structures, which act as nucleation scaffolds for the remaining diffusing filaments and bundles. (a) By virtue of their longer length, WT filaments rapidly form more extensive arrested structures, which recruit the remaining filaments and bundles into a broader-ranging network structure. On the other hand (b), shorter filaments of the phosphomimicry mutants, with a larger percolation threshold in relation to the WT system, form shorter-ranging arrested structures, which results in the more weakly-connected and characteristic node-like mutant network structure. (For interpretation of the references to colour in this figure legend, the reader is referred to the web version of this article.)

The variability in network structure as a function of concentration shows how the constituent concentration affects the outcome of the structural arrest. WT bundled networks at 20 μM have an observed mesh size ≈3 μm, much larger than the <0.5 μm measured for networks of keratin filaments [29], further demonstrating the contribution of the kinetic arrest component within the network assembly scheme. Moreover, reducing the median filament length results in an increase in filament number (per mass of protein), which in the absence of (interaction-driven) structural arrest would be expected to assemble into networks with a tighter mesh; yet the Ser → Glu system pairs assemble into networks with larger mesh sizes. The inverse relation of protein concentration to mesh size could explain how transfected Ser → Glu plasmids do not produce *de facto* disrupted networks: an *in vivo* concentration of keratins ≈500 μM [21] is high enough to mask the observation of prestress network differences to the WT. We report on the mechanical outcome of the mutation-induced structural changes. We show that bundling enables the network to withstand much higher stresses with smaller resulting deformations, which matches *in vivo* observations whereby shear stress-dependent remodeling of the keratin network is characterized by an increase in bundle formation [10,22].

Combining the structural and the mechanical data enables us to suggest a framework for keratin network growth and development, Fig. 7, and the mechanism with which phosphorylation is involved in its modification. Beyond ULF elongation into the mature filament, the interplay of filament arrest and bundling modulates the resultant network structure, both of which are diffusion-limited and governed by filament association through the rod domain. The spatially-extended and slower-diffusing WT filaments associate into a more extensive arrested structure (pink contoured structure in Fig. 7), which is thus further slowed-down and serves as a nucleation scaffold for the remaining filaments and bundles. On the other hand, the shorter and faster-diffusing mutant filaments associate into lesser-spanning and more sparsely distributed nodes (color contoured structures in Fig. 7), whereby the discrepancy in diffusion timescales between the mutant filaments and their corresponding arrested structures is smaller than that for the WT system. The arrested structures also serve to limit bundle growth by sterically limiting the accessibility of the arrested components. This steric hindrance is additional cause for the structural discrepancy between the Ser → Glu and the WT networks: the less extended arrested Ser → Glu structures provide a lower steric barrier, enabling the Ser → Glu protein nodes to grow more laterally, enabling clustering and further dampening the ability to produce a more extensive network. The network structure schematically depicted in Fig. 7 represents the local properties, which translate to the entire network.

5. Conclusions

Phosphorylation of keratins has previously been shown to increase their solubility *in vivo*, creating a rapidly diffusing pool, essential for the delivery of keratins to their nucleation sites [4], and to affect their binding to associated proteins, namely the 14-3-3 protein group [4,26]. Though binding of keratins to other proteins has been implicated in the rearrangement of the keratin protein network, we show that keratins alone and upon phosphorylation are able to achieve this reordering. The structural modularity of the keratin network is made possible by the non-equilibrium nature of keratin network construction, and is put into effect by the existence of multiple orders of self-assembly, propagating the constituent attributes to the macroscopic framework. The filament-to-filament attractions drive bundle formation and subsequent structural arrest of contacting network components, whereby varying constituent filament length produces bundles and arrested structures with differing morphologies. We show how the reduction in filament length due to phosphorylation mediates the sequestering of soft epithelial keratins into lesser-connected components, and enables the network to exhibit much larger deformability. In a physiological context, phosphorylation allows the same quantity of material to be rapidly reconfigured by depleting initial connectivity, altering the structural framework to meet the changing needs of the cell. Characterizing such kinetic arrest contributions to cytoskeletal biopolymer assembly is critical to understanding their structure and function relationship.

Author contributions

J.D. and A.R.B. designed research; J.D., F.H., L.R., and K.W. performed research; J.D., F.H., and A.R.B. analyzed data; J.D. and A.R.B. wrote paper; F.H. and L.R. commented on manuscript.

Additional information

The authors declare no competing financial interests.

Acknowledgments

We gratefully acknowledge the support by the Deutsches Forschungsgemeinschaft (DFG) through the SFB863 and the Nanosystems Initiative Munich (NIM).

JD is also grateful to the TUM University Foundation and the Alexander von Humboldt Foundation for their postdoctoral fellowship support.

Appendix A. Supplementary data

Supplementary data associated with this article can be found, in the online version, at http://dx.doi.org/10.1016/j.actbio.2016.07.010.

References

[1] P.A. Coulombe, P. Wong, Cytoplasmic intermediate filaments revealed as dynamic and multipurpose scaffolds, Nat. Cell Biol. 6 (2004) 699–706.
[2] E. Fuchs, K. Weber, Intermediate filaments: structure, dynamics, function, and disease, Annu. Rev. Biochem. 63 (1994) 345–382.
[3] L.M. Godsel, R.P. Hobbs, K.J. Green, Intermediate filament assembly: dynamics to disease, Trends Cell Biol. 18 (2008) 28–37.
[4] R. Windoffer, M. Beil, T.M. Magin, R.E. Leube, Cytoskeleton in motion: the dynamics of keratin intermediate filaments in epithelia, J. Cell Biol. 194 (2011) 669–678.
[5] N.T. Snider, M.B. Omary, Post-translational modifications of intermediate filament proteins: mechanisms and functions, Nat. Rev. Mol. Cell Biol. 15 (2014) 163–177.
[6] N.O. Ku, S. Azhar, M.B. Omary, Keratin 8 phosphorylation by p38 kinase regulates cellular keratin filament reorganization: modulation by a keratin 1-like disease causing mutation, J. Biol. Chem. 277 (2002) 10775–10782.
[7] N.O. Ku, M.B. Omary, Identification of the major physiologic phosphorylation site of human keratin 18: potential kinases and a role in filament reorganization, J. Cell Biol. 127 (1994) 161–171.
[8] N.O. Ku, M.B. Omary, Phosphorylation of human keratin 8 in vivo at conserved head domain serine 23 and at epidermal growth factor-stimulated tail domain serine 431, J. Biol. Chem. 272 (1997) 7556–7564.
[9] M.B. Omary, N.O. Ku, G.Z. Tao, D.M. Toivola, J. Liao, "Heads and tails" of intermediate filament phosphorylation: multiple sites and functional insights, Trends Biochem. Sci. 31 (2006) 383–394.
[10] S. Sivaramakrishnan, J.L. Schneider, A. Sitikov, R.D. Goldman, K.M. Ridge, Shear stress induced reorganization of the keratin intermediate filament network requires phosphorylation by protein kinase C ζ, Mol. Biol. Cell. 20 (2009) 2755–2765.
[11] H. Herrmann, M. Haner, M. Brettel, N.O. Ku, U. Aebi, Characterization of distinct early assembly units of different intermediate filament proteins, J. Mol. Biol. 286 (1999) 1403–1420.

[12] H. Herrmann, T. Wedig, R.M. Porter, E.B. Lane, U. Aebi, Characterization of early assembly intermediates of recombinant human keratins, J. Struct. Biol. 137 (2002) 82–96.
[13] T. Lichtenstern, N. Mucke, U. Aebi, M. Mauermann, H. Herrmann, Complex formation and kinetics of filament assembly exhibited by the simple epithelial keratins K8 and K18, J. Struct. Biol. 177 (2012) 54–62.
[14] J. Block, V. Schroeder, P. Pawelzyk, N. Willenbacher, S. Koster, Physical properties of cytoplasmic intermediate filaments, Biochim. Biophys. Acta 2015 (1853) 3053–3064.
[15] C.Y.J. Hémonnot, M. Mauermann, H. Herrmann, S. Köster, Assembly of simple epithelial keratin filaments: deciphering the ion dependence in filament organization, Biomacromolecules 16 (2015) 3313–3321.
[16] J. Kayser, H. Grabmayr, M. Harasim, H. Herrmann, A.R. Bausch, Assembly kinetics determine the structure of keratin networks, Soft Matter 8 (2012) 8873–8879.
[17] C.H. Lee, P.A. Coulombe, Self-organization of keratin intermediate filaments into cross-linked networks, J. Cell Biol. 186 (2009) 409–421.
[18] A.K. Wilson, P.A. Coulombe, E. Fuchs, The roles of K5 and K14 head, tail, and R/K L L E G E domains in keratin filament assembly in vitro, J. Cell Biol. 119 (1992) 401–414.
[19] S. Yamada, D. Wirtz, P.A. Coulombe, Pairwise assembly determines the intrinsic potential for self-organization and mechanical properties of keratin filaments, Mol. Biol. Cell. 13 (2002) 382–391.
[20] J.F. Nolting, W. Mobius, S. Koster, Mechanics of individual keratin bundles in living cells, Biophys. J. 107 (2014) 2693–2699.
[21] X. Feng, H. Zhang, J.B. Margolick, P.A. Coulombe, Keratin intracellular concentration revisited: implications for keratin function in surface epithelia, J. Invest. Dermatol. 133 (2013) 850–853.
[22] E.W. Flitney, E.R. Kuczmarski, S.A. Adam, R.D. Goldman, Insights into the mechanical properties of epithelial cells: the effects of shear stress on the assembly and remodeling of keratin intermediate filaments, FASEB J. 23 (2009) 2110–2119.
[23] M. Beuttenmuller, M. Chen, A. Janetzko, S. Kuhn, P. Traub, Structural elements of the amino-terminal head domain of vimentin essential for intermediate filament formation in vivo and in vitro, Exp. Cell Res. 213 (1994) 128–142.
[24] L.H. Gu, P.A. Coulombe, Defining the properties of the nonhelical tail domain in type II keratin 5: insight from a bullous disease-causing mutation, Mol. Biol. Cell. 16 (2005) 1427–1438.
[25] M. Hatzfeld, M. Burba, Function of type I and type II keratin head domains: their role in dimer, tetramer and filament formation, J. Cell Sci. 107 (1994) 1959–1972.
[26] N.O. Ku, S. Michie, E.Z. Resurreccion, R.L. Broome, M.B. Omary, Keratin binding to 14-3-3 proteins modulates keratin filaments and hepatocyte mitotic progression, Proc. Natl. Acad. Sci. U.S.A. 99 (2002) 4373–4378.
[27] S. Winheim, A.R. Hieb, M. Silbermann, E.M. Surmann, T. Wedig, H. Herrmann, J. Langowski, N. Mücke, Deconstructing the late phase of vimentin assembly by total internal reflection fluorescence microscopy (TIRFM), PLoS One 6 (2011).
[28] D. Wildanger, E. Rittweger, L. Kastrup, S.W. Hell, STED microscopy with a supercontinuum laser source, Opt. Express 16 (2008) 9614–9621.
[29] P. Pawelzyk, N. Mucke, H. Herrmann, N. Willenbacher, Attractive interactions among intermediate filaments determine network mechanics in vitro, PLoS One 9 (2014) e93194.
[30] K.M. Schmoller, O. Lieleg, A.R. Bausch, Structural and viscoelastic properties of actin/filamin networks: cross-linked versus bundled networks, Biophys. J. 97 (2009) 83–89.
[31] J.S. Kim, C.-H. Lee, P.A. Coulombe, Modeling the self-organization property of keratin intermediate filaments, Biophys. J. 99 (2010) 2748–2756.
[32] L. Ma, S. Yamada, D. Wirtz, P.A. Coulombe, A 'hot-spot' mutation alters the mechanical properties of keratin filament networks, Nat. Cell Biol. 3 (2001) 503–506.
[33] P. Pawelzyk, H. Herrmann, N. Willenbacher, Mechanics of intermediate filament networks assembled from keratins K8 and K18, Soft Matter 9 (2013) 8871–8880.
[34] S. Yamada, D. Wirtz, P.A. Coulombe, The mechanical properties of simple epithelial keratins 8 and 18: discriminating between interfacial and bulk elasticities, J. Struct. Biol. 143 (2003) 45–55.
[35] D.W. Owens, N.J. Wilson, A.J. Hill, E.L. Rugg, R.M. Porter, A.M. Hutcheson, R.A. Quinlan, D. van Heel, M. Parkes, D.P. Jewell, S.S. Campbell, S. Ghosh, J. Satsangi, E.B. Lane, Human keratin 8 mutations that disturb filament assembly observed in inflammatory bowel disease patients, J. Cell Sci. 117 (2004) 1989–1999.